Grid cells in rat entorhinal cortex encode physical space with independent firing fields and phase precession at the single-trial level

Eric T. Reifenstein[a,b], Richard Kempter[b], Susanne Schreiber[b], Martin B. Stemmler[a], and Andreas V. M. Herz[a,1]

[a]Department of Biology II, Ludwig-Maximilians-Universität München, and Bernstein Center for Computational Neuroscience Munich, 82152 Planegg-Martinsried, Germany; and [b]Institute for Theoretical Biology, Humboldt-Universität zu Berlin, and Bernstein Center for Computational Neuroscience Berlin, 10115 Berlin, Germany

Edited* by John J. Hopfield, Princeton University, Princeton, NJ, and approved March 08, 2012 (received for review June 14, 2011)

When a rat moves, grid cells in its entorhinal cortex become active in multiple regions of the external world that form a hexagonal lattice. As the animal traverses one such "firing field," spikes tend to occur at successively earlier theta phases of the local field potential. This phenomenon is called phase precession. Here, we show that spike phases provide 80% more spatial information than spike counts and that they improve position estimates from single neurons down to a few centimeters. To understand what limits the resolution and how variable spike phases are across different field traversals, we analyze spike trains run by run. We find that the multiple firing fields of a grid cell operate as independent elements for encoding physical space. In addition, phase precession is significantly stronger than the pooled-run data suggest. Despite the inherent stochasticity of grid-cell firing, phase precession is therefore a robust phenomenon at the single-trial level, making a theta-phase code for spatial navigation feasible.

neural coding | spatial representation | spike-timing code | oscillator-interference model

Finding and remembering paths to follow through an environment relies on specialized neural circuits in which subgroups of neurons encode different spatial locations. A spatial region that causes a cell to fire spikes defines a "firing field"; for instance, place cells in CA1 of hippocampus often have a single firing field, whereas grid cells in the medial entorhinal cortex (mEC) have multiple, regularly spaced firing fields that are arranged in hexagonal grids (1–5).

Spatial location is represented not only in the firing rates of such cells (Fig. 1*A*), but also in the timing of spikes relative to global rhythms in the network (Fig. 1*B*). A prominent 6- to 11-Hz network oscillation—the "theta rhythm"—modulates the firing patterns of nerve cells throughout the entire entorhinal–hippocampal formation during exploratory behavior and accompanies the spatial periodicity of rodent grid cells (6, 7). By adding up the spikes recorded on many runs of the rodent through the same firing field, Hafting et al. (8) observed a pattern of progressively earlier phases relative to the theta rhythm for the spikes of layer II mEC grid cells. This phenomenon is termed phase precession and was first described in place cells from the hippocampus (9–12).

The observation that spatial position correlates negatively with the average phase of spikes does not answer the question of whether the animal can use this phenomenon for estimating its location at the single-run level. In fact, not only could the average, pooled behavior mask the variability of phase precession in single runs, but even more drastically, single-run phase precession could be unrelated to pooled phase precession. For instance, single runs could exhibit no or only little phase precession, whereas pooled runs would exhibit phase precession (Fig. 1*C*). The spikes on single runs could even recess in phase, yet still lead to phase precession in the pooled data. Single-run phase precession could also be stronger than the pooled runs suggest (Fig. 1*D*). Moreover, runs with strong phase precession could be interspersed with runs in which the spikes lock to a particular theta phase of the local field potential (LFP). There is also another aspect of grid-cell activity that needs to be taken into account: From one firing field to the next one visited, the discharge of a single grid cell may or may not be correlated. Hence it is an open question whether the nervous system can actually make use of phase coding in mEC, notwithstanding the trends seen in pooled data or at the single-run level in hippocampal place cells (13).

Results

Extracellularly isolated cells from layer II medial entorhinal cortex and the LFP were recorded by Hafting et al. (8) from rats running along a linear track, and made available by E. I. Moser (Norwegian University of Science and Technology, Trondheim, Norway). Many cells had multiple firing fields, corresponding to different locations at which the cell spiked (Fig. 1*A*). To analyze the relationship between the timing of spikes and the background theta rhythm in the LFP, we computed an instantaneous theta phase of the LFP by taking the Hilbert transform of the LFP signal, band-passed between 6 and 11 Hz. During the traversal of a single grid field, the firing rate first rises and then falls (Fig. 1*A*). At the same time, the average spike phase relative to the ongoing theta rhythm decreases (Fig. 1*B*). Hence, both the phase and the number of spikes within a theta cycle are a function of the rat's position within the firing field.

To quantify phase precession, regression analyses were performed. Because phase is a circular variable, traditional linear correlation analysis, as in Hafting et al. (8), may yield slope and correlation estimates that do not reflect the true structure in the data (Fig. S1). Therefore, we turned to circular–linear methods (14, 15). Indeed, the median linear correlation for a set of 291 grid fields from 67 cells, pooled across runs for each field, is found to be -0.28 ± 0.02, whereas the median circular–linear correlation coefficient is only -0.05 ± 0.04.

Such weak correlations could imply that the theta phase of spikes in single entorhinal grid cells is not a reliable indicator of spatial location, so we asked how well the phase of spikes relative to the theta LFP predicts the rat's position compared with the spike count. For any single run through a given location, the number and phase of a grid cell's spikes varies. By pooling over different runs through a grid field, we map the joint probability distribution of the rat's position and either the spike count or the spike phase (Fig. 2 *A* and *B*). Kernel density methods yield smoothed estimates for these distributions (*Materials and Methods*). In the example of Fig. 2*A*,

Author contributions: E.T.R., R.K., S.S., M.B.S., and A.V.M.H. designed research; E.T.R. performed research; E.T.R., M.B.S., and A.V.M.H. analyzed data; and E.T.R., R.K., S.S., M.B.S., and A.V.M.H. wrote the paper.

The authors declare no conflict of interest.

*This Direct Submission article had a prearranged editor.

Freely available online through the PNAS open access option.

[1]To whom correspondence should be addressed. E-mail: herz@bio.lmu.de.

This article contains supporting information online at www.pnas.org/lookup/suppl/doi:10.1073/pnas.1109599109/-/DCSupplemental.

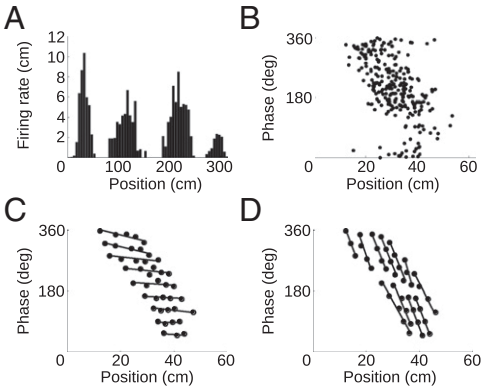

Fig. 1. The animal's position within the firing field modulates both the firing rate and theta phase. (*A*) Average firing rate of a grid cell for a rat running 42 times from left to right along a linear track. (*B*) The phase relative to the ongoing theta rhythm of all spikes from the leftmost grid field in *A*. Each dot depicts a single spike. (*C* and *D*) Hypothetical cases for which the relationship between the spike phase and the animal's position differs radically between single runs and pooled-run data. (*C*) Example in which spikes tend to be phase locked to the LFP oscillation, so that all subsequent spikes in later theta cycles follow at about the same phase as the initial spike. If the phase of the initial spike depends on the spatial coordinate, then the pooled-run data can mimic phase precession. (*D*) Phase precession in single runs can also be stronger than suggested by pooled data. Pooled phase precession in *C* and *D* is identical and could thus belie the phase–position relationship in single runs.

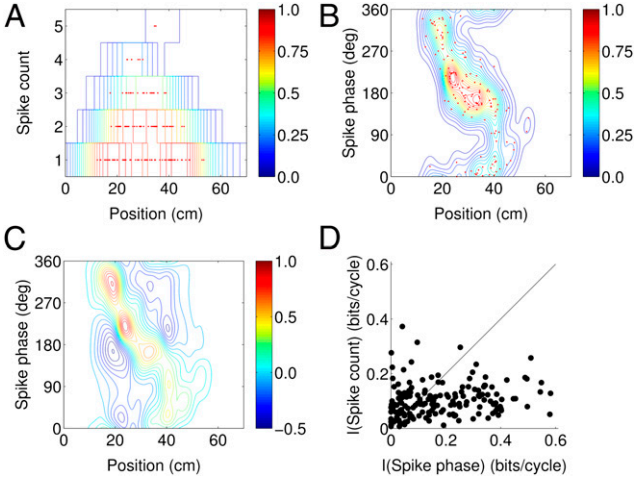

Fig. 2. The phase of spikes relative to the theta rhythm and the spike count per theta period convey spatial information. (*A*) Smoothed probability density of the position and the spike count in a theta cycle, $p_{X,N}(x,n)$, obtained by kernel density estimation (*Materials and Methods*) for the grid field depicted in Fig. 1*B*. The probability density (color bar) is normalized relative to the maximum value. Observed counts are indicated by red dots. (*B*) Normalized joint probability density of the position and phase of spikes relative to its theta cycle, $p_{X,\Theta}(x,\theta)$, for the same grid field. Red dots depict the phase of the first spike in each theta cycle, measured across different theta cycles and different runs. The average phase decreases as a function of position, whereas the spike count's relationship to position is inherently ambiguous: for instance, the average spike count at $x \approx 20$ cm$(\bar{n} \approx 1.75)$ is nearly the same as that at $x \approx 40$ cm$(\bar{n} \approx 1.65)$, whereas the (circular) average phases are 285° and 104°, respectively. (*C*) The difference $p_{X,\Theta}(x,\theta) - p_X(x)p_\Theta(\theta)$ reflects the strong correlation between phase and position induced by precession. (*D*) Theta phase conveys more information about position than does spike count ($p < 0.001$), as demonstrated by compound data from all grid fields (n = 166).

the most likely number of spikes within a theta cycle, given that the grid cell spiked at all, was always one, regardless of the rat's position within the grid field. Higher numbers of spikes only occurred toward the center of the grid field. Likewise, any particular location on the linear track leads to a specific range of possible phases for the first spikes within a theta cycle (Fig. 2*B*).

To quantify the effect of these uncertainties, we estimated the information the two different spike measures convey about the position. If position and phase were statistically independent, for instance, their joint probability $p_{X,\Theta}(x,\theta)$ would be equal to the product of the marginal probability distributions, $p_X(x)p_\Theta(\theta)$; Fig. 2*C* shows that this is not the case. Here, the joint probability clearly exceeds the product of the marginals along a negatively slanted diagonal throughout the grid field.

Different positions within a grid field map onto different expected spike phases; however, firing rates rise toward the center and then fall again, so that generally two positions are associated with the same average spike count. This ambiguity implies additional uncertainty, reducing the information available in the spike count to about half of that contained in the spike phase (0.102 ± 0.005 vs. 0.18 ± 0.01 bits/cycle). On a grid field-by-grid field basis, too, phase conveys more information about position than spike count ($P < 0.001$; Fig. 2*D*).

How precisely can one estimate the rat's position from the theta phase or spike count? A lower bound on the accuracy can be given by estimating the Fisher information (see Materials and Methods) using the kernel density estimates of the probability distributions. On average, the spike count allows one to discriminate nearby positions down to 9.3 ± 0.6 cm, whereas the theta phase differentiates positions to an accuracy of 5.8 ± 0.6 cm, i.e., about 1/10th of the grid field's size (56.0 ± 1.2 cm).

Information measures based on pooled data, however, reveal nothing about spatial encoding in single runs. For instance, the phase precession shown schematically in Fig. 1 *C* and *D* would yield the same average information between position and phase. A run-by-run analysis is warranted.

Just how few spikes participate in phase precession can be appreciated by a closer examination of single runs. In over half the runs, fewer than five spikes were elicited. Often, spikes on a single run reflect a nearly linear progression of phase with position (Fig. 3*A*); in some cases, connecting the spikes by lines in the phase vs. position diagram reveals a zigzag pattern in which one or more spikes follow the leading spike in a given theta cycle (Fig. 3*B*). Such "follower" spikes within the same theta cycle amount to about one-half of all spikes and occur with highly variable phase delays that can be >90°. After removing these unreliable spikes and considering only the leading spikes, a clearer signature of phase precession emerges (Fig. 3 *C* and *D*), even though the median number of spikes drops from five to three (Fig. 3*E*).

The median correlation in single runs is −0.33 ± 0.03 for leading spikes, compared with −0.24 ± 0.02 for all spikes (Fig. 3*F*, n = 5,948 runs with more than two leading spikes), although the distribution of correlation values is extremely broad; in fact, all possible correlation values from −1 to +1 are observed (Fig. 3*G*). The average slope, which measures the theta phase shift per distance traveled, changes from a mean value of −9.6 ± 0.1 degrees (deg)/cm for all spikes to −11.1 ± 0.1 deg/cm for the leading spikes (Fig. 3*H*; n = 5,948). The SD of either underlying distribution is large: 11.7 deg/cm for all spikes and 9.3 deg/cm for the leading spikes (Fig. 3*I*). Nonetheless, the difference in the mean slope of 1.5 deg/cm is highly significant ($P < 10^{-5}$).

Pooling can conceal the properties of phase precession during single runs. Comparing the pooled leading spikes to the leading spikes on single runs, the median correlation coefficient in many grid fields is more negative on single runs (Fig. 4*A*; $P < 0.001$). Apart from the inherent variability manifest in Fig. 3, the schematic of Fig. 1*D*, therefore, resembles phase precession on single runs: the average phase slope is about 30% more negative and significantly less variable than the pooled slope (Fig. 4*B*; paired t test: $P < 0.001$).

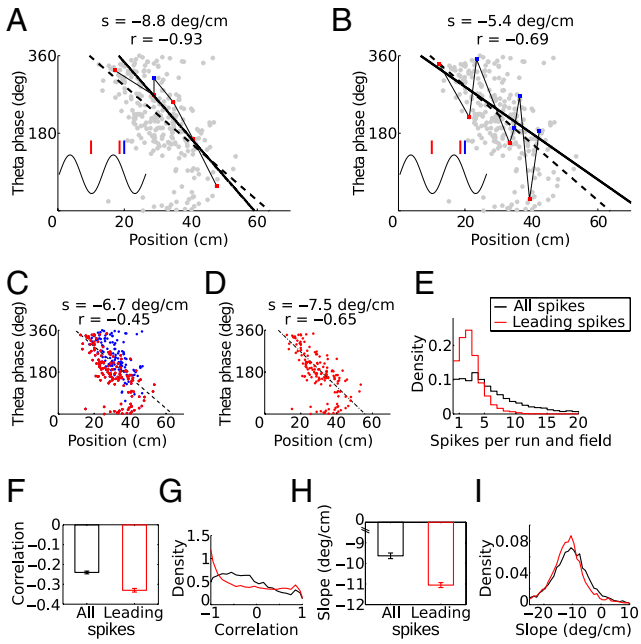

Fig. 3. Phase precession in single runs through grid fields. In each run, multiple theta cycles occur within a grid field. (*A* and *B*) Two typical single runs (red and blue squares connected by thin solid line; red squares, leading spikes; blue squares, later spikes within the same theta cycle, as sketched in the *Insets*) through the grid field shown in Figs. 1 and 2. Solid lines depict the circular fit to the single runs; dashed lines depict circular fit to all runs. Spikes from other runs through the grid field are shown in light gray. The slope *s* and the correlation coefficient *r* are given above the graphs. (*C*) Regression fit to all spikes across all runs through the grid field. (*D*) Regression fit to all of the leading spikes within each theta cycle of this grid field, after discarding any later spikes within the same cycle. (*E*) Histograms of spike counts per single run and grid field for all firing fields and grid cells (black line, median: 5) and for only the leading spikes (red line, median: 3). (*F*) Median circular correlation coefficient of all spikes and of leading spikes on single runs (-0.24 ± 0.02 vs. -0.33 ± 0.03). (*G*) Histograms of single-run correlation coefficients for all spikes (black line) and for leading spikes (red line). The two distributions are significantly different (Kolmogorov–Smirnov test: $P < 0.001$). (*H*) Slopes of circular fits for all spikes in a single run and for leading spikes (-9.6 ± 0.1 vs. -11.1 ± 0.1 deg/cm). (*I*) Histogram of the slopes fitted to all spikes and to only leading spikes. Some 9.7% of the slopes fall outside of the range shown. The two distributions differ significantly from one another (Kolmogorov–Smirnov test: $P < 0.001$).

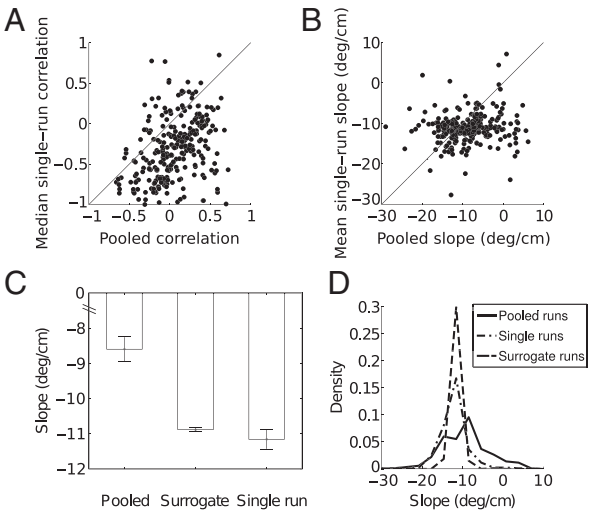

Fig. 4. Pooling spikes across runs distorts salient features of phase precession. Shown are results for the leading spikes in each theta cycle; averaged data from a single grid field are denoted by a dot. (*A*) The median single-run phase–position correlation is more negative than the pooled-data correlation (Wilcoxon rank-sum test: $p < 10^{-5}$, $n = 291$). (*B*) The mean single-run slope is less variable than the pooled slope (paired *t* test: $p < 10^{-5}$). (*C*) The phase changes ~30% more rapidly with position in single runs than predicted by the pooled runs, yielding a steeper slope (-11.2 ± 0.3 vs. -8.6 ± 0.3 deg/cm, averaged per grid field, not per run). The slopes of artificial, surrogate single runs (-10.9 ± 0.1 deg/cm) and actual runs are not significantly different. Surrogate single runs for a grid field were created by drawing leading spikes from the pooled data of that field, and the number of spikes in surrogate runs matched the number of spikes in the actual runs. (*D*) Circular regression of phase vs. position is more variable across grid fields if multiple runs are pooled first. The SD in the slope of pooled phase precession is 6.0 deg/cm, compared with 4.7 deg/cm in the mean slope of single runs.

To test whether the changes in the correlation coefficients and slopes of phase precession could be explained by the low number of leading spikes in single runs, we drew surrogate runs at random from the pooled data of leading spikes, using the same spike-count distribution as in the actual single runs. For each grid field ($n = 291$), we computed the median circular phase–position correlation in surrogate and actual single runs, as before. The median of the median correlations in surrogate and actual single runs was $r = -0.29 \pm 0.02$ and $r = -0.34 \pm 0.05$, respectively. Per grid field, the phase precessed at -10.9 ± 0.1 deg/cm in surrogate single runs, and at -11.2 ± 0.3 deg/cm in the actual single runs (Fig. 4*C*); though the mean values were not significantly different, the underlying distributions for the slopes differed between surrogate and actual runs (Fig. 4*D*).

Remarkably, the mean single-run slopes are less variable across grid fields than the pooled-data slopes across grid fields (Fig. 4*D*): 4.7 deg/cm (SD) for single runs vs. 6.0 deg/cm. In particular, the pooled data for some grid fields show no phase precession or even phase recession (zero or positive slope in the phase vs. position diagram). However, with the exception of four grid fields, the majority of single runs always precessed (Fig. 4*B*).

Unlike the firing fields of place cells, grid fields regularly repeat. If phase precession codes the animal's position, instead of being just a side effect of the theta rhythm, we need to investigate whether neural activity in one field depends on activity in the field visited previously (Fig. 5). Across runs, we compared the phase of the first spike in the present field with the phase of specific spikes in the prior field: the first spike (Fig. 5*B*), the last leading spike (Fig. 5*C*), or the last spike (Fig. 5*D*). For all three combinations, the joint probabilities were indistinguishable from the product of the respective marginal distributions, as shown by a generalized Kolmogorov–Smirnov test ($P = 0.83$, $P = 0.74$, $P = 0.74$, respectively; *Materials and Methods*). Similarly, neither the number of spikes ($P = 0.81$), nor the leading spike count ($P = 0.99$), nor the phase-precession slopes (all spikes: $P = 0.94$, leading spikes: $P = 0.94$) exhibited any significant field-to-field dependencies on single runs. We also asked whether phase precession in the next field is simply an extension of the precession in the previous field, as forecast by elementary oscillator-interference models for the generation of grid fields (16). Extrapolating the regression line fitted to one field failed to predict the phase of the first spike in the next field, however (Fig. 5 *E* and *F*; circular correlation $r = 0.01$, $P = 0.64$). The same was true when we also took the number of elapsed theta cycles into account (circular correlation $r = -0.01$, $P = 0.64$). To reveal subtle effects that might not have been captured by the above analyses, we finally tested whether single-run deviations from the mean response in each field (measured as the phase of the first spike, phase-precession slope, spike count, leading spike count, or leading spike slope) were correlated along the rat's track, but did not find any significant trends (circular correlation $r = 0.015$, $P =$

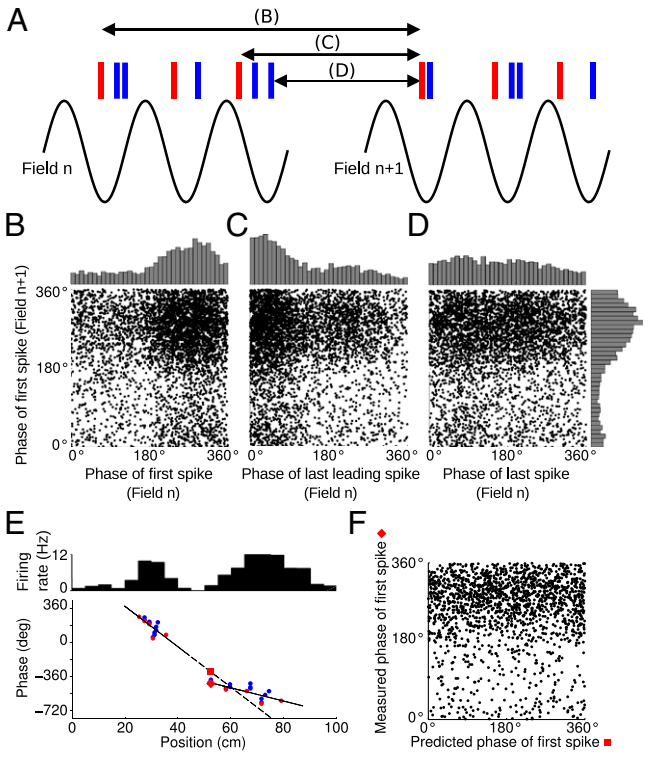

Fig. 5. Relation between successive firing fields of a grid cell. (*A*) The first-spike phase in field $n + 1$ (*Right*) could depend on various parameters of the cell's activity in field n (*Left*), such as the phase of the first spike, phase of the last leading spike, or phase of the last spike. As in Fig. 3, leading spikes are drawn in red, followers in blue. (*B–D*) The corresponding joint-probability distributions together with the respective marginal probabilities. The product structure of the joint-probability distributions indicates that the individual firing fields of one grid cell operate as independent encoders of physical space. In line with this observation, phase precession in one field does not predict the phase of the first spike in the next field, as illustrated in *E* and evidenced by population data (*F*).

0.31; Pearson's $r = 0.01$, $P = 0.53$; Pearson's $r = -0.02$, $P = 0.09$; Pearson's $r = 0.002$, $P = 0.89$; Pearson's $r = -0.002$, $P = 0.99$; respectively). Together, these findings indicate that the different firing fields of a grid cell provide independent information to downstream processing stages in the hippocampus.

Discussion

The negative correlation between a rat's location and the theta phase of grid-cell spikes (8, 17) invites the conjecture that the animal's brain works with these phases to navigate through the environment. This conjecture is at the core of various computational models (10, 16, 18) but had not been tested on experimental data. In the present analysis, we used the spike trains from single entorhinal grid cells recorded by Hafting et al. (8) to estimate the spatial information conveyed by theta phase and spike count, and studied the differences between single runs and pooled runs through grid fields as well as relations between individual grid fields.

Given the trial-to-trial variability of the theta phase of spikes throughout the entorhinal–hippocampal complex, one needs to prove that the phase contains useful information about the animal's position. This task is not always trivial: for an ensemble of simultaneously recorded, phase-precessing neurons in hippocampal CA1, Jensen and Lisman (19) used a Bayesian reconstruction algorithm to show that adding phase information improves the spatial resolution more than simply using the firing rate, narrowing the uncertainty from 4 cm to 3 cm under ideal conditions. However, an earlier study found that including the phases in the reconstruction algorithm led to no improvement (20).

For grid cells, firing fields repeat in a regular pattern. The spike phase of a single cell yields an instantaneous position estimate that is local and unique up to the intrinsic length scale of the grid. The coherence of the ongoing theta rhythm and cell-intrinsic mechanisms might induce dependencies between the discharge patterns evoked in different grid fields of the same cell. Our analysis shows that this is not the case (Fig. 5), and that each firing field of a grid cell can be regarded as an independent encoder of physical space. Because the animals were moving rapidly, passing through successive grid fields within as few as 10 theta cycles, this is a surprising result. Our finding suggests that the neural noise level is small enough to enable single-run phase-precession patterns within a grid field, yet large enough to decorrelate the activity from field to field. This interpretation is in accordance with in-vitro data (21) that show that EC stellate cells generate stochastic sub-threshold membrane potential oscillations whose low coherence may be responsible for the fast decorrelations observed in vivo.

As grid fields independently encode position in the phase, each one can be considered in isolation, so that we can estimate probability distributions for position and phase from pooling multiple runs through individual grid fields. Here, we found that the spike count within a theta cycle resolved the rat's position within a grid field to an average accuracy of 9.3 cm, whereas the spike phases improves that value to 5.8 cm, only little more than 1/10th of the mean grid-field size of 56 cm.

Phase precession on single grid-field traversals differed qualitatively from the average phase precession obtained by pooling many runs. In single runs, the change in phase with distance traveled was more pronounced, and the measured correlation between position and phase was more negative. Using surrogate data to take sample-size effects into account revealed that both observations are compatible with the reduced number of spikes in single runs. We conclude that phase precession is clearly present in the behaviorally relevant situation and that traditional pooling underestimates its strength by ∼30%.

In the hippocampal CA1 region, the correlations between phase and position also tend to be more negative on single runs (13). A cardinal difference between entorhinal grid cells and hippocampal place cells exists, however: inside a CA1 cell's place field, bursts frequently occur within theta cycles; a grid cell, in contrast, fires comparatively few bursts. The median number of spikes elicited during the traversal of a place field is ten (13), much higher than the five spikes in a grid field. Nonetheless, the leading spike in each theta cycle yielded a clear signature of phase precession in mEC. These leading spikes might be effective triggers of spiking activity in other areas—a much longer time delay (median: 92 ms) precedes them, compared with the delay that precedes follower spikes (median: 12 ms), so that the effect of leading spikes will be less prone to synaptic depression and adaptation downstream. Phase precession in place cells could thus be inherited from the phase precession of the leading spikes in mEC. Assuming that precisely timed activity of multiple grid cells is required to fire a single place cell, one might expect a reduction of the single-run phase range from EC to hippocampus. Indeed, the median single-run phase precession in entorhinal grid cells is 250°, whereas Schmidt et al. (13) observe that phase precession in CA1 during single runs typically extends over 180°, or half the full range of phases from 0° to 360° encompassed by pooled-run data.

Phase-precession measures in mEC grid cells were highly variable across single runs (Fig. 3 *F–I*), and the same phenomenon is observed in CA1 place cells. Information quantifies the uncertainty induced by variability, without pinpointing the source of uncertainty. Intrinsic noise, spike time jitter, and the LFP itself all contribute.

Population rhythms sculpt the timing of spikes (22–24), yet the LFP's theta phase is not synchronized to the location of the rat: at the moment when the rat enters a grid field, the theta phase is different on every run. In contrast, the oscillation phase in visual and auditory cortex is consistent in response to repeated

presentations of the same stimulus (25, 26). Cells throughout the mEC show a preference for spiking at particular phases of the theta and gamma rhythm in the LFP (17, 27); precession implies that the preferred phase shifts as the rat traverses the cell's firing field. The difference between the initial phase upon grid field entry and the preferred phase for spiking will affect when, and hence where, a grid cell will spike first. As a consequence, the pooled portrait of phase precession can be interpreted as the sum of the steeper phase precession sequences on individual runs; on each run, the line of phase precession is subject to a variable lateral shift along the position axis. Four factors, however, complicate this simple picture. First, single-run phase precession is not only steeper, on average, but also highly variable. Second, many entorhinal grid cells skip different theta cycles on different runs (27, 28). Third, the theta band LFP itself is noisy and not perfectly coherent in time. Fourth, any coupling to the gamma-band LFP will also shift the timing of grid cell spikes and thereby perturb the map between theta phase and the rat's position.

As the wide-range synchrony in the theta LFP organizes the spiking across different neurons (28), the single-run characteristics of phase precession, including the field-to-field independence, become decisive, and not the averaged precession properties derived from pooling over multiple runs. Indeed, firing sequences in simultaneously recorded place cells in CA1 have been shown to be more highly structured than predicted from the pooled, average phase–position relationship (29); the same may hold true for simultaneously recorded grid cells in mEC, but this remains to be seen.

Materials and Methods

Both published and previously unpublished data recorded by Hafting et al. (8) were reanalyzed (http://www.ntnu.no/cbm/moser/gridcell). In these experiments, grid cells were recorded extracellularly from layer II in the mEC of eight rats that ran on a linear track (length: 320 cm). Data include single-unit activity, the LFP sampled at a frequency of 250 Hz, and the position of the rat, as tracked by a diode fixed to the animal's head (8).

For our analysis, the spikes on each run were partitioned into firing fields, using the same criteria as Hafting et al. (8). Grid fields on runs from left to right were not generally the same as grid fields on runs in the reverse direction, and so were treated separately. Runs from right to left were mirrored for the data analysis, so that fields are always entered from the left and exited on the right. A total of 291 grid fields from 67 units were analyzed. Unlike Hafting et al. (8), we did not exclude fields with low spatial coherence between neighboring bins. In total, there were 9,561 single runs. The number of single runs per grid field ranged from 6 to 97. The raw LFP signal was filtered in the theta range (6–11 Hz). Using the Hilbert transform of the filtered signal, every spike was assigned an instantaneous theta phase. Two sets of spikes were considered: (*i*) the set of all spikes in a grid field and (*ii*) only the first spikes in each theta cycle (these spikes were termed leading spikes). In these two sets, there were 66,365 and 31,734 spikes, respectively. The phase precession properties associated with the leading spikes also held for other methods of choosing a single spike within a theta cycle (e.g., the average or the last spike in each theta cycle).

Phase precession was quantified by two measures (13–15): the slope s from circular–linear regression, which results from fitting the model $\theta = s \cdot (x - x_0)$ to the data by maximizing

$$R = \sqrt{\left(\frac{1}{n}\sum_{i=1}^{n}\cos(\theta_i - sx_i)\right)^2 + \left(\frac{1}{n}\sum_{i=1}^{n}\sin(\theta_i - sx_i)\right)^2},$$

and the circular–linear correlation coefficient

$$r = \frac{\sum_i \sin(\theta_i - \bar{\theta})\sin(\varphi_i - \bar{\varphi})}{\sqrt{\sum_i \sin^2(\theta_i - \bar{\theta})\sum_j \sin^2(\varphi_j - \bar{\varphi})}},$$

where θ_i denotes the theta phase of the i-th spike, $\varphi_i = s \cdot x_i \bmod 2\pi$ is a circular variable that is derived from the animal's position x_i, and $\bar{\varphi} = \arg\left(\frac{1}{n}\sum_{j=1}^{n}\exp(i\varphi_j)\right)$ and $\bar{\theta} = \arg\left(\frac{1}{n}\sum_{j=1}^{n}\exp(i\theta_j)\right)$ are the circular sample mean values (14).

Linear–linear correlation (30) is inherently ambiguous, because phase is a circular variable. Typically, one adds a phase offset to all spike phases in a given grid field and searches for the offset that leads to the largest (absolute) correlation. As a consequence of the optimization step, the estimated linear–linear correlation coefficient is nonzero, even if phase and position are completely uncorrelated (14, 15). When sample sizes are small, this effect is exacerbated. In contrast, the median circular–linear correlation coefficient is independent of any phase offset and is much more conservative, yielding lower values for the correlation coefficients, as also observed by Huxter et al. (31) in CA1. Fig. S1 compares the values of the linear–linear and circular–linear fits across all grid fields in the data set. The circular–linear slopes provided a better visual match to the data and were much steeper, on average, than the original mean value of -2.77 ± 0.31 deg/cm (8), which was derived by averaging across linear regressions.

The statistical likelihood of observing specific properties of phase precession in single runs was estimated by drawing surrogate runs from the pooled data. Each spike is associated with a position and a phase, so that the set of all (position, phase) pairs from actual runs is $\{(x_i, \theta_i)\}$. For each true run, a surrogate run with the same number of spikes was created, drawing the position and phase for each spike randomly from $\{(x_i, \theta_i)\}$ without replacement.

Mutual information is used to estimate how well the rat's position is encoded in the theta phase of action potentials or in the spike count within individual theta cycles. For two random variables, X and Φ, the mutual information is defined as

$$I(\Phi, X) = \iint_{\Phi,X} p_{\Phi,X}(\varphi, x)\log\left(\frac{p_{\Phi,X}(\varphi, x)}{p_\Phi(\varphi)p_X(x)}\right)d\varphi dx,$$

where $p_{\Phi,X}(\varphi, x)$ denotes the joint probability density of the two random variables, and $p_\Phi(\varphi)$ and $p_x(x)$ are the marginal probability densities.

Whereas the mutual information reflects the global uncertainty about one random variable, given the other random variable, the Fisher information, defined as

$$I_F(x) = \int_\Phi p_{\Phi|X}(\varphi|x)\left(\frac{\partial}{\partial x}\log p_{\Phi|X}(\varphi|x)\right)^2 d\varphi,$$

measures the local uncertainty. Here, $p_{\Phi|X}(\varphi|x)$ is the conditional probability of observing a theta-based variable φ given a position x. It can be shown that the variance of any unbiased estimator is bounded from below by the Cramér–Rao inequality

$$\sigma_x^2 \geq \frac{1}{I_F(x)}.$$

Though an ideal observer can, in many instances, construct an estimator that reaches the lower bound, it should be stressed that not all estimators are ideal (20), and that we measure the theoretical resolution limit. Both information measures require knowledge of the underlying probability distributions. Because the data are finitely sampled, the distributions can only be approximated. For this purpose, we use the kernel density estimation method described by Botev et al. (32). The number of measured spikes was sufficient to estimate the probability density in 166 grid fields.

Unless stated otherwise, the SEM is used as the measure of uncertainty. To test for significance, we generally used two-sample two-tailed t tests, testing for equal means of the two data samples. Because correlation coefficients turned out to stem from strongly skewed distributions, median values are given together with their 95% confidence intervals. The Wilcoxon rank-sum test was used to test whether the medians of two sets of sampled correlation data were the same. To test whether two data samples stem from the same underlying distribution, the Kolmogorov–Smirnov test was applied. Its 2D extension due to Fasano and Franceschini (33) tested for potential field-to-field dependencies by comparing the measured joint probability distribution with the product distribution obtained from the respective marginals. Here, mean P values were obtained from 100 data shuffles. In general, the P value indicates the likelihood of observing a result that is as least as extreme as the one that was actually observed, assuming that the null hypothesis (equal means, equal medians, or same distribution, respectively) is true. $P < 0.05$ was considered significant.

ACKNOWLEDGMENTS. We thank E. I. Moser and coworkers for their hospitality to E.T.R, and for making data recorded by T. Hafting and coworkers publicly available; science benefits greatly when such altruistic data-sharing occurs. We also thank C. Kluger, A. Mathis, R. Schmidt, and K. Thurley for stimulating discussions. This work was supported by Deutsche Forschungsgemeinschaft Grants SFB 618 and GRK 1123, and German Federal Ministry for Education and Research Grants 01GQ0440, 01GQ0901, 01GQ0972, and 01GQ1001A.

1. Fyhn M, Molden S, Witter MP, Moser EI, Moser MB (2004) Spatial representation in the entorhinal cortex. *Science* 305:1258–1264.
2. Hafting T, Fyhn M, Molden S, Moser MB, Moser EI (2005) Microstructure of a spatial map in the entorhinal cortex. *Nature* 436:801–806.
3. Barry C, Hayman R, Burgess N, Jeffery KJ (2007) Experience-dependent rescaling of entorhinal grids. *Nat Neurosci* 10:682–684.
4. Moser EI, Kropff E, Moser MB (2008) Place cells, grid cells, and the brain's spatial representation system. *Annu Rev Neurosci* 31:69–89.
5. Boccara CN, et al. (2010) Grid cells in pre- and parasubiculum. *Nat Neurosci* 13: 987–994.
6. Brandon MP, et al. (2011) Reduction of theta rhythm dissociates grid cell spatial periodicity from directional tuning. *Science* 332:595–599.
7. Koenig J, Linder AN, Leutgeb JK, Leutgeb S (2011) The spatial periodicity of grid cells is not sustained during reduced theta oscillations. *Science* 332:592–595.
8. Hafting T, Fyhn M, Bonnevie T, Moser MB, Moser EI (2008) Hippocampus-independent phase precession in entorhinal grid cells. *Nature* 453:1248–1252.
9. O'Keefe J, Recce ML (1993) Phase relationship between hippocampal place units and the EEG theta rhythm. *Hippocampus* 3:317–330.
10. Skaggs WE, McNaughton BL, Wilson MA, Barnes CA (1996) Theta phase precession in hippocampal neuronal populations and the compression of temporal sequences. *Hippocampus* 6:149–172.
11. Harris KD, et al. (2002) Spike train dynamics predicts theta-related phase precession in hippocampal pyramidal cells. *Nature* 417:738–741.
12. Huxter J, Burgess N, O'Keefe J (2003) Independent rate and temporal coding in hippocampal pyramidal cells. *Nature* 425:828–832.
13. Schmidt R, et al. (2009) Single-trial phase precession in the hippocampus. *J Neurosci* 29:13232–13241.
14. Jammalamadaka SR, SenGupta A (2001) *Topics in Circular Statistics* (World Scientific, Singapore).
15. Kempter R, Leibold C, Buzsáki G, Diba, K, Schmidt R (2012) Quantifying circular-linear associations: Hippocampal phase precession. *J Neurosci Meth*, in press.
16. Burgess N, Barry C, O'Keefe J (2007) An oscillatory interference model of grid cell firing. *Hippocampus* 17:801–812.
17. Mizuseki K, Sirota A, Pastalkova E, Buzsáki G (2009) Theta oscillations provide temporal windows for local circuit computation in the entorhinal-hippocampal loop. *Neuron* 64:267–280.
18. Kamondi A, Acsády L, Wang XJ, Buzsáki G (1998) Theta oscillations in somata and dendrites of hippocampal pyramidal cells in vivo: Activity-dependent phase-precession of action potentials. *Hippocampus* 8:244–261.
19. Jensen O, Lisman JE (2000) Position reconstruction from an ensemble of hippocampal place cells: Contribution of theta phase coding. *J Neurophysiol* 83:2602–2609.
20. Zhang K, Ginzburg I, McNaughton BL, Sejnowski TJ (1998) Interpreting neuronal population activity by reconstruction: Unified framework with application to hippocampal place cells. *J Neurophysiol* 79:1017–1044.
21. Erchova I, Kreck G, Heinemann U, Herz AVM (2004) Dynamics of rat entorhinal cortex layer II and III cells: characteristics of membrane potential resonance at rest predict oscillation properties near threshold. *J Physiol* 560:89–110.
22. Chrobak JJ, Buzsáki G (1998) Gamma oscillations in the entorhinal cortex of the freely behaving rat. *J Neurosci* 18:388–398.
23. Lisman J (2005) The theta/gamma discrete phase code occurring during the hippocampal phase precession may be a more general brain coding scheme. *Hippocampus* 15:913–922.
24. Whittingstall K, Logothetis NK (2009) Frequency-band coupling in surface EEG reflects spiking activity in monkey visual cortex. *Neuron* 64:281–289.
25. Montemurro MA, Rasch MJ, Murayama Y, Logothetis NK, Panzeri S (2008) Phase-of-firing coding of natural visual stimuli in primary visual cortex. *Curr Biol* 18:375–380.
26. Kayser C, Montemurro MA, Logothetis NK, Panzeri S (2009) Spike-phase coding boosts and stabilizes information carried by spatial and temporal spike patterns. *Neuron* 61:597–608.
27. Deshmukh SS, Yoganarasimha D, Voicu H, Knierim JJ (2010) Theta modulation in the medial and the lateral entorhinal cortices. *J Neurophysiol* 104:994–1006.
28. Quilichini P, Sirota A, Buzsáki G (2010) Intrinsic circuit organization and theta-gamma oscillation dynamics in the entorhinal cortex of the rat. *J Neurosci* 30:11128–11142.
29. Foster DJ, Wilson MA (2007) Hippocampal theta sequences. *Hippocampus* 17: 1093–1099.
30. Mehta MR, Lee AK, Wilson MA (2002) Role of experience and oscillations in transforming a rate code into a temporal code. *Nature* 417:741–746.
31. Huxter JR, Senior TJ, Allen K, Csicsvari J (2008) Theta phase-specific codes for two-dimensional position, trajectory and heading in the hippocampus. *Nat Neurosci* 11: 587–594.
32. Botev ZI, Grotowski JF, Kroese DP (2010) Kernel density estimation via diffusion. *Ann Stat* 38:2916–2957.
33. Fasano G, Franceschini A (1987) A multidimensional version of the Kolmogorov–Smirnov test. *Mon Not R Astron Soc* 225:155–170.